(12) LEVEL III

DNA 4700F

ELF PROPAGATION UNDER DISTURBED CONDITIONS

Comparison of Theory With Available Data

E. C. Field
Pacific-Sierra Research Corp.
1456 Cloverfield Blvd.
Santa Monica, California 90404

1 December 1978

Final Report for Period 1 November 1976—1 December 1978

CONTRACT No. DNA 001-77-C-0039

APPROVED FOR PUBLIC RELEASE;
DISTRIBUTION UNLIMITED.

THIS WORK SPONSORED BY THE DEFENSE NUCLEAR AGENCY
UNDER RDT&E RMSS CODE B322077464 S99QAXHB04218 H2590D.

Prepared for
Director
DEFENSE NUCLEAR AGENCY
Washington, D. C. 20305

BLANK PAGES
IN THIS
DOCUMENT
WERE NOT
FILMED

Destroy this report when it is no longer needed. Do not return to sender.

PLEASE NOTIFY THE DEFENSE NUCLEAR AGENCY, ATTN: TISI, WASHINGTON, D.C. 20305, IF YOUR ADDRESS IS INCORRECT, IF YOU WISH TO BE DELETED FROM THE DISTRIBUTION LIST, OR IF THE ADDRESSEE IS NO LONGER EMPLOYED BY YOUR ORGANIZATION.

DNA PRINTING PLANT

UNCLASSIFIED

SECURITY CLASSIFICATION OF THIS PAGE *(When Data Entered)*

REPORT DOCUMENTATION PAGE		READ INSTRUCTIONS BEFORE COMPLETING FORM
1. REPORT NUMBER DNA 4700F	2. GOVT ACCESSION NO.	3. RECIPIENT'S CATALOG NUMBER
4. TITLE *(and Subtitle)* ELF PROPAGATION UNDER DISTURBED CONDITIONS Comparison of Theory With Available Data		5. TYPE OF REPORT & PERIOD COVERED Final Report for Period 1 Nov 76—1 Dec 78 6. PERFORMING ORG. REPORT NUMBER PSR-813
7. AUTHOR(s) E. C. Field		8. CONTRACT OR GRANT NUMBER(s) DNA 001-77-C-0039
9. PERFORMING ORGANIZATION NAME AND ADDRESS Pacific-Sierra Research Corp. 1456 Cloverfield Blvd. Santa Monica, California 90404		10. PROGRAM ELEMENT, PROJECT, TASK AREA & WORK UNIT NUMBERS Subtask S99QAXHB042-18
11. CONTROLLING OFFICE NAME AND ADDRESS Director Defense Nuclear Agency Washington, D.C. 20305		12. REPORT DATE 1 December 1978 13. NUMBER OF PAGES 58
14. MONITORING AGENCY NAME & ADDRESS*(if different from Controlling Office)*		15. SECURITY CLASS *(of this report)* UNCLASSIFIED 15a. DECLASSIFICATION/DOWNGRADING SCHEDULE

16. DISTRIBUTION STATEMENT *(of this Report)*

Approved for public release; distribution unlimited. 62704H

17. DISTRIBUTION STATEMENT *(of the abstract entered in Block 20, if different from Report)*

18. SUPPLEMENTARY NOTES

This work sponsored by the Defense Nuclear Agency under RDT&E RMSS Code B322077464 S99QAXHB04218 H2590D.

19. KEY WORDS *(Continue on reverse side if necessary and identify by block number)*

Submarine Communications
ELF Blackout
Ionospheric Disturbances

20. ABSTRACT *(Continue on reverse side if necessary and identify by block number)*

An extensive literature survey has identified a number of low-frequency noise measurements relevant to the effects of ionospheric disturbances on ELF propagation. These measurements pertain to the behavior of earth-ionosphere cavity resonances and ELF/VLF noise intensity at the time of 1) the Starfish high-altitude nuclear detonation, 2) more than thirty solar flares, and 3) two polar-cap-absorption events (PCAs). Until controlled-source ELF experiments are carried out under disturbed conditions, these collateral data provide the

DD FORM 1 JAN 73 1473 EDITION OF 1 NOV 65 IS OBSOLETE

UNCLASSIFIED

SECURITY CLASSIFICATION OF THIS PAGE *(When Data Entered)*

20. ABSTRACT (Continued)

only means by which codes that predict ELF propagation in nuclear environments can be compared with experiment.

A full-wave propagation code similar to predictive codes developed under DNA auspices is used to compute ELF propagation anomalies due to Starfish, PCA events, and a large number of model x-ray flares. The results of these calculations are compared—to the extent possible—to the available data. Despite the inadequacies of the data, we are able to verify key theoretical predictions.

Good agreement is demonstrated between code predictions and ELF/VLF noise intensity during solar flares. Both experiment and theory consistently show that the vast majority of flares cause the intensity to increase at frequencies between 30Hz and 1 kHz, decrease between 5 kHz and 10 kHz, and increase between 10 kHz and 30 kHz. This agreement, which occurs over three frequency decades, strongly implies the correctness of the predictive codes.

Although the Schumann-resonance band (8-to-30 Hz) is somewhat lower than the ELF communications band (45-to-80 Hz), both bands propagate in the TEM waveguide mode. Data on Schumann resonances may therefore be meaningfully compared with the outputs of ELF propagation codes. The results of such a comparison made in this report semiquantitatively support the validity of the codes. Specifically, the numerical calculations correctly predict that either Starfish or the PCAs would cause the peak frequencies of the Schumann resonances to shift downward by 0.5 Hz to 1 Hz and the Q's of the resonances to decrease. The shift in resonant frequencies is due to the depressed ionosphere causing the phase velocity of the signal to decrease and the decrease in Q is caused by an increase in the attenuation rate in the earth-ionosphere waveguide.

SUMMARY

An extensive literature survey has identified a number of low-frequency noise measurements relevant to the effects of ionospheric disturbances on ELF propagation. These measurements pertain to the behavior of earth-ionosphere cavity resonances and ELF/VLF noise intensity at the time of 1) the Starfish high-altitude nuclear detonation, 2) more than thirty solar flares, and 3) two polar-cap-absorption events (PCAs). Until controlled-source ELF experiments are carried out under disturbed conditions, these collateral data provide the only means by which codes that predict ELF propagation in nuclear environments can be compared with experiment.

A full-wave propagation code similar to predictive codes developed under DNA auspices is used to compute ELF propagation anomalies due to Starfish, PCA events, and a large number of model x-ray flares. The results of these calculations are compared--to the extent possible--to the available data. Despite the inadequacies of the data, we are able to verify key theoretical predictions.

Good agreement is demonstrated between code predictions and ELF/VLF noise intensity during solar flares. Both experiment and theory consistently show that the vast majority of flares cause the intensity to increase at frequencies between 30 Hz and 1 kHz, decrease between 5 kHz and 10 kHz, and increase between 10 kHz and 30 kHz. This agreement, which occurs over three frequency decades, strongly implies the correctness of the predictive codes.

Although the Schumann-resonance band (8-to-30 Hz) is somewhat lower than the ELF communications band (45-to-80 Hz), both bands propagate in the TEM waveguide mode. Data on Schumann resonances may therefore be meaningfully compared with the outputs of ELF propagation codes. The results of such a

comparison made in this report semiquantitatively support the validity of the codes. Specifically, the numerical calculations correctly predict that either Starfish or the PCAs would cause the peak frequencies of the Schumann resonances to shift downward by 0.5 Hz to 1 Hz and the Q's of the resonances to decrease. The shift in resonant frequencies is due to the depressed ionosphere causing the phase velocity of the signal to decrease and the decrease in Q is caused by an increase in the attenuation rate in the earth-ionosphere waveguide.

PREFACE

The goal of this report is to verify, insofar as is possible, codes that predict ELF propagation in nuclear environments. An extensive literature search is made to assemble atmospheric noise measurements relevant to ELF propagation during ionospheric disturbances. These data are compared with calculations made using existing ELF propagation codes.

TABLE OF CONTENTS

LIST OF FIGURES

LIST OF TABLES

I. INTRODUCTION

It is frequently asserted that the ability of current theory to predict the performance of ELF communications systems in nuclear environments is unproven because relevant experimental data do not exist. Strictly speaking, such assertions are true because no experiment using a controlled ELF source in a nuclear environment has ever been performed, nor is one likely to be performed so long as the test-ban treaty remains in force. Moreover, no data have been obtained on transpolar signals from a controlled ELF source during a major polar-cap-absorption (PCA) event, which would exhibit some of the characteristics of a nuclear environment.

Accordingly, this report gives the results of a program to use collateral data from low-frequency noise measurements to verify--insofar as it is possible--the ability of current codes to predict the effects of ionospheric disturbances on received ELF signal strength. Obviously, this approach has severe limitations, and the results cannot be expected to be as satisfactory as would those obtained from dedicated experiments using controlled sources. Nonetheless, as discussed below, it does prove possible to verify semiquantitatively some important predictions of existing codes.

An important aspect of the research described in this report is an extensive literature survey to accumulate data relevant to the excitation and propagation of ELF signals under disturbed conditions. The most useful of the data reviewed are measurements of ELF/VLF atmospheric noise intensity and the structure of the earth-cavity (Schumann) resonances during the Starfish high-altitude nuclear test, several PCA events, and numerous sudden ionospheric disturbances (SIDs). We do not consider in detail data from the Wisconsin Test Facility ELF transmitter, which have been adequately addressed by other investigators (e.g., *Imhoff, et al., 1976*).

Section II reviews the salient aspects of ELF propagation theory and codes based thereon and establishes the applicability of these codes to Schumann resonance phenomena; Sec. III summarizes the data accumulated during the literature search; Sec. IV presents computational results and compares them with the data given in Sec. III; Sec. V summarizes the conclusions.

II. LONG-WAVE PROPAGATION CODES

This section briefly summarizes some important aspects of currently used long-wave propagation codes and establishes the applicability of these codes to the interpretation of measurements of ELF/VLF atmospheric noise and the Schumann resonances.

ELF/VLF PROPAGATION

The detailed equations governing ELF/VLF propagation in the earth-ionosphere waveguide are given in a number of references (e.g., *Budden, 1961, Field, 1970; Pappert and Moler, 1974; Field, Lewinstein, and Dore, 1976*), and will not be repeated here. These references, among others, also describe the numerical procedures employed by current ELF/VLF codes to solve these equations. These codes account for the vertical inhomogeneity of the ionosphere, the horizontal inhomogeneity of the ionosphere along the great-circle connecting transmitter and receiver, and the curvature of the earth; but neglect horizontal inhomogeneities transverse to the great-circle path. Field (*1978*) considers the effects of transverse inhomogeneities and gives a correction term to be used if the transverse dimension of an ionospheric disturbance is smaller than a Fresnel zone. To define symbols and illustrate key dependences, the equation for the spatial dependence of ELF/VLF fields is given and discussed below.

Usually, somewhat different equations are used for ELF and VLF propagation because the WTF ELF antenna is horizontally oriented, whereas most operational VLF transmitters are vertically oriented. Here, however, we are concerned with atmospheric noise generated by the vertical component of lightning strokes, and a single equation may therefore be used. In general, only one waveguide mode--the TEM mode--can propagate at ELF;

but several modes can contribute to VLF fields. In this report, we restrict attention to long paths, so that higher modes are heavily attenuated, and only a single VLF mode--the TM-1 mode--need be considered.

Subject to the above conditions, the following equation describes the vertical electric field at both ELF and VLF:

$$E = -120\pi i e^{-\pi i/4} \frac{IL}{\sqrt{\lambda d}} \sqrt{\frac{d/a}{\sin d/a}} \; S^{3/2} \Lambda e^{-\beta d/(8.7 \times 10^6)} \; e^{-(2\pi i/\lambda)(c/v)} \; V/M \quad . \quad (1)$$

In Eq. (1), IL is the effective electric dipole moment of the source, λ is the free-space wavelength, d is the distance from source to receiver, a is the earth's radius, and c is the vacuum speed of light. MKS units are used except where expressly indicated otherwise.

The role of propagation codes is to determine the dependence of the signal, E, on the state of the ionosphere. This dependence occurs solely through two quantities: 1) the excitation factor, Λ, which governs the efficiency with which the waveguide mode is generated; 2) the quantity, S, which is essentially the eigenvalue of the relevant waveguide mode. The losses suffered by a signal as it propagates in the earth-ionosphere waveguide are given by the attenuation rate, β, which is expressed in decibels of loss per megameter of propagation (dB/Mm). The phase velocity of the signal is denoted by v. Both β and v are related to S by the following simple relations:

$$S \equiv S_R + i\, S_i \quad , \quad (2)$$

$$\beta = 0.18\, f\, S_i \quad dB/Mm \quad , \quad (3)$$

$$c/v = S_R \quad , \quad (4)$$

where f is the wave frequency.

The quantity actually computed by long-wave propagation codes is the so-called eigencosine, C, of the relevant waveguide mode. The closely related quantity, S, is then obtained from

$$S = \sqrt{1 - C^2} \quad . \tag{5}$$

This distinction between C and S is important in the verification of codes because S_R and S_i are the quantities that can be determined experimentally, whereas C is the quantity actually computed. The main point--especially at ELF, where neither the real nor the imaginary part of C is particularly small--is that S_R depends strongly on *both* C_R *and* C_i. Thus, the correctness of a calculated value of S_R (phase velocity) implies a correct value of S_i (attenuation rate), and vice-versa.

The above discussion shows that output of a long-wave propagation code is essentially two quantities, A and S, and that verification should involve comparison of measured value of these quantities with calculated results. This procedure is vastly more complicated than indicated by the apparently simple equations. The calculation of S requires a highly sophisticated iterative numerical technique that uses detailed profiles of ionospheric charged-particle densities and collision frequencies as inputs. Moreover, nature is seldom so cooperative as to provide a uniform propagation path characterized by a single value of S at all locations. Thus, even if transverse ionospheric variations can be ignored, measured ELF data pertain to a propagation path along which various ionospheric profiles and ground conductivities are encountered.

Finally, we note that, although all equations given in this section are formally valid at both ELF and VLF, implicit differences exist between the two bands. For frequencies below about 1 kHz, the eigenvalue S and

excitation factor Λ correspond to the TEM mode, which has a somewhat different structure than the TM-1 mode, to which S and Λ correspond above a few kilohertz. However, the numerical procedures used to calculate S and Λ are identical for these two modes.

APPLICABILITY TO SCHUMANN-RESONANCE DATA

The equations given above are in a form applicable to ELF communications frequencies of many tens of hertz, for which the wavelength is much smaller than the circumference of the earth. Some of the most useful of the available data were measured in the so-called Schumann resonance band. This band includes frequencies between about 8 Hz and 30 Hz, which are somewhat lower than frequencies usually associated with ELF communications. Electromagentic signals at 8-to-30 Hz propagate in the same TEM mode as do 45-to-80-Hz ELF communications signals, and essentially the same theoretical treatment applies equally well to the two bands. Thus, a validation of code predictions in the Schumann band strongly implies that predictions in the usual ELF band are also correct. However, because wavelengths in the Schumann band can be comparable to the earth's circumference, it is convenient to write the equation for the electric field in a form that differs somewhat from Eq. (1).

Galejs (*1972*) shows that the vertical electric field is given by

$$E \approx \frac{iIL}{8\pi f \varepsilon_o h a^2} \frac{(kaS)^2}{\cos(\pi kaS)} P_\nu(-\cos d/a) \quad \text{v/m} \quad , \tag{6}$$

where P is the Legendre function, k is the free-space wave number, h is the nominal reflection height of the ionosphere, and the approximation

$$\nu = \sqrt{0.25 + (kaS)^2} - \tfrac{1}{2} \quad , \tag{7a}$$

$$\approx kaS - \tfrac{1}{2} \tag{7b}$$

has been made. Equation (6) is actually more accurate at all frequencies than Eq. (1), which is an approximate form convenient for use at frequencies higher than about 30 Hz. Specifically, by using the large-order asymptotic expansion of P_ν, neglecting waves that travel around the earth more than once, noting that $\Lambda \approx 1/h$, and performing some algebraic manipulation, it is straightforward (but tedious) to show that Eq. (6) may be approximated by Eq. (1)--provided that the wavelength is much smaller than the earth's circumference.

Equation (6) shows that the spectrum of background noise would be expected to exhibit peaks near frequencies where the denominator exhibits minima; viz., spectral peaks should occur where

$$\cos(\pi kaS) = \text{minimum} \quad . \tag{8}$$

Equation (8) will be satisfied at a series of n complex frequencies given by (n = 1, 2, ---)

$$\tilde{f}_n = f_n + i f_{in} = \frac{(n+\tfrac{1}{2})c}{2\pi aS} \quad \text{Hz} \quad . \tag{9}$$

Thus, the center frequency of the n^{th} resonant peak is given by

$$f_n \approx \frac{(n+\tfrac{1}{2})c}{2\pi\, a\, S_R} \quad \text{Hz} \quad , \tag{10}$$

and the "Q" of the n^{th} peak is given by

$$Q_n \equiv \frac{f_n}{2f_{in}} \approx \frac{S_R}{2S_i} \quad . \tag{11}$$

In Eqs. (10) and (11), use has been made of the fact that $S_i^2 << S_R^2$. Recall that Q_n is a measure of the width of a resonant peak and becomes smaller if the peak becomes wider; i.e., if the peak is "smeared." If the earth and ionosphere were sharply bounded perfect conductors, S_R would equal unity, and Eq. (10) would predict resonances at 10.6 Hz, 18.3 Hz, 25.9 Hz, etc. Calculations using realistic ionospheres, however, show that S_R is somewhat larger than unity, reducing the predicted resonant frequencies to around 8 Hz, 14 Hz, 20 Hz, 26 Hz, etc., under ambient conditions. Figure 1 shows a nominal measured noise-power spectrum, similar to that first measured by Balser and Wagner (*1960*). The theoretically predicted peaks are evident.

Schumann resonances are particularly convenient for interpretation because f_n and Q_n depend solely on S_R and S_i, which essentially are the phase velocity and attenuation rate of the signal (see Eqs. (3) and (4)). Thus, unlike measurements of noise intensity that depend on source strength and excitation factor, measured values of f_n depend to a good approximation *solely* on the phase velocity, and thus present no ambiguity in interpretation.

The goal of this report is to establish--insofar as is possible--that currently used codes correctly predict ELF signal changes associated with ionospheric disturbances. Specifically, a change in ionospheric structure will cause Λ and S to assume new post-disturbance values, denoted by $\Lambda + \Delta\Lambda$ and $S + \Delta S$. In a strong nuclear environment, ΔS_i is so large as to create a severe increase in the attenuation rate β, thus causing blackout. For the disturbances of natural origin considered in Secs. III and IV below,

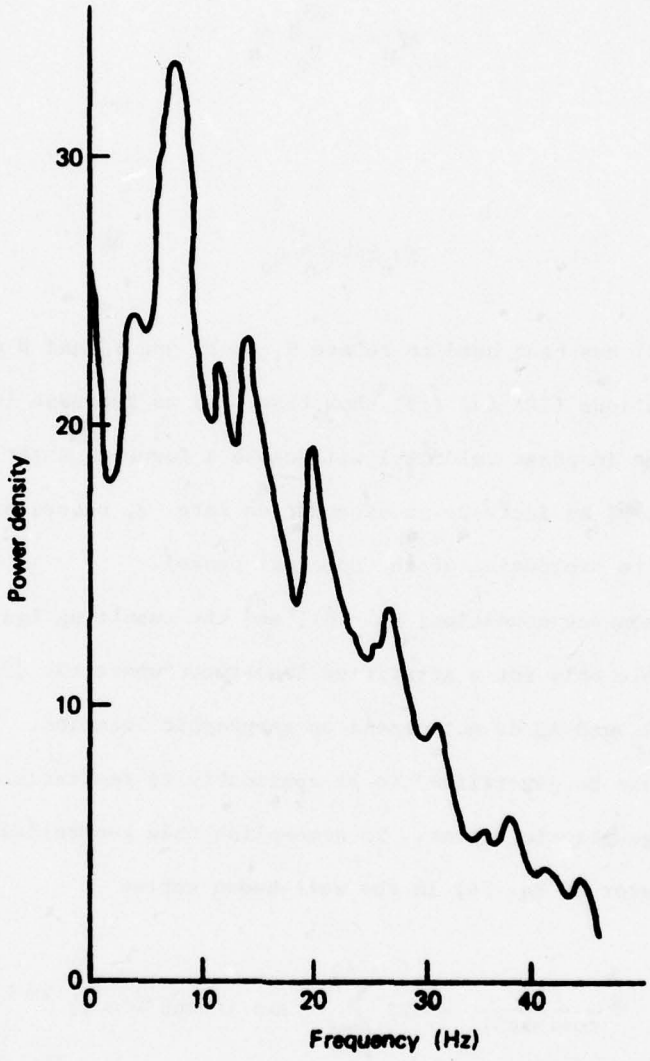

Fig. 1--Typical measured power spectrum of atmospheric noise in the 0-to-40-Hz band. Note the resonances at around 8 Hz, 14 Hz, 20 Hz, etc.

it is valid to assume $\Delta S << S$; and it follows from Eqs. (10) and (11) that

$$\Delta f_n \simeq - \frac{\Delta S_R}{S_R} f_n \quad , \tag{12}$$

and

$$\Delta Q_n \approx - \frac{\Delta \beta}{\beta} Q_n \quad , \tag{13}$$

where Eq. (3) has been used to relate S_i to β, and S_R and β are evaluated at f_n. Equations (12) and (13) show that: a) an increase in S_R (equivalent to a decrease in phase velocity) will cause a downward shift in the resonant frequencies; b) an increase in attenuation rate, β, causes a reduction in Q (equivalent to broadening of the spectral peaks).

The resonance condition, Eq. (8), and the resulting Eqs. (12) and (13) are applicable only for a stratified ionosphere where the disturbance is such that ΔS_R and $\Delta\beta$ do not depend on geographic location. Thus, these equations must be generalized to be applicable to realistic disturbances of limited geographic extent. To accomplish this generalization, we expand the denominator of Eq. (6) in the well-known series

$$\frac{1}{\cos(\pi kaS)} = 2i \sum_{m=0}^{\infty} \exp i(\pi kaS - \pi/2)^{2m+1} \quad . \tag{14}$$

Note that πa is the distance a wave travels in propagating halfway around the earth, and πkaS is the phase change corresponding to this distance. It is therefore evident from Eq. (14) that Schumann resonances occur from the constructive self-interference of waves that travel around the earth a

large number of times, while undergoing a $\pi/2$ phase change each time the antipode is passed. The resonance condition, (Eq. (8)), simply defines the discrete frequencies for which the phase term πkaS assures that a wave will constructively self-interfere after having made an integer number of round trips.

The best available data on the effects of ionospheric disturbances on Schumann resonances were taken during the Starfish high-altitude nuclear test and several PCA events. The resulting disturbances--although not worldwide--were far from being localized. Under these conditions, it is reasonable to use the phase-memory approximation, and note that the phase, Φ, corresponding to propagation from source to antipode can be written

$$\Phi = \pi ka\left[S + \frac{1}{\pi}\int_0^{\pi} d\theta \Delta S(\theta)\right] \text{ radians} \quad , \tag{15}$$

where θ is the usual angular spherical coordinate and the integral is taken along the great-circle path containing source and receiver. Thus, the effective value of the perturbation on S is

$$\langle \Delta S \rangle = \frac{1}{\pi}\int_0^{\pi} d\theta \Delta S(\theta) \quad , \tag{16}$$

where $\langle \Delta S \rangle$ is the average value of ΔS taken over the path. By substituting $S + \langle \Delta S \rangle$ for S in the resonance condition, Eq. (8), it is easily shown that Eqs. (12) and (13) become

$$\Delta f_n \simeq -\frac{\langle \Delta S_R \rangle}{S_R} f_n \quad , \tag{17}$$

and

$$\Delta Q_n \simeq - \frac{\langle \Delta\beta \rangle}{\beta} \, Q_n \quad . \tag{18}$$

If good data were available on the location of sources and lateral ionospheric structure at the time of the measured disturbances, it would be reasonable to perform full-fledged calculations of the average values $\langle \Delta S_R \rangle$ and $\langle \Delta\beta \rangle$ indicated in Eqs. (17) and (18). Unfortunately, the data summarized in Sec. III are much too coarse to warrant a complex calculation, and there is no choice but to use rather crude estimates for $\langle \Delta S_R \rangle$ and $\langle \Delta\beta \rangle$. Specifically, we use

$$\langle \Delta S_R \rangle \approx F \Delta S_R$$

$$\langle \Delta\beta \rangle \approx F \Delta\beta \quad ,$$

where ΔS_R and $\Delta\beta$ are taken to be characteristic values along the path containing source and receiver and extending the circumference of the earth, and F denotes the estimated fraction of this path over which these characteristic values obtain. The final, very approximate, form of the equations used to relate ionospheric disturbances to changes in Schumann resonances thus becomes

$$\Delta f_n \simeq - \frac{F \Delta S_R}{S_R} \, f_n \tag{19}$$

$$\Delta Q_n \simeq - \frac{F \Delta\beta}{\beta} \, Q_n \quad . \tag{20}$$

III. SUMMARY OF AVAILABLE DATA

This section summarizes the results of a literature survey to assemble data pertinent to the effects of ionospheric disturbances on ELF signal strength. As indicated in Sec. II, the behavior of Schumann resonances during ionospheric disturbances is relevant to the verification of ELF predictive codes, although Schumann resonance frequencies are lower than those under consideration for ELF communications. Therefore, this section gives Schumann resonance data as well as data for the behavior of ELF noise intensity during various types of disturbances. In some situations, VLF noise data were taken in conjunction with ELF noise data, thus affording an opportunity to interpret the relative behavior of both bands. Thus, although this report is concerned with verification of theoretical predictions at ELF, some VLF data are given, where appropriate.

NOISE INTENSITY MEASUREMENTS

Effects of X-Ray Flares

Scientists from Japan have carried out two measurement programs to determine the change in intensity of background ELF/VLF noise caused by solar x-ray flares. The first set of measurements, made in May 1963, monitored ELF frequencies of 30 Hz, 100 Hz, 260 Hz, and 600 Hz; and VLF frequencies of 10 kHz, 21 kHz, and 27 kHz (*Sao and Jindoh, 1966*). The results of those measurements are shown in Table 1, which presents the change in noise intensity that occurred at the onset of four flares. Note that, in almost every instance, the noise intensity increased somewhat, motivating the term SEA (sudden enhancement of atmospherics) to describe the phenomenon.

The second set of measurements, made during 1968 and 1969, was much more extensive than the first (*Sao, et al., 1970*). More than 20 events were monitored, and more frequencies (100 Hz, 170 Hz, 260 Hz, 400 Hz, 570 Hz, 800 Hz at ELF; 5 kHz, 10 kHz, 21 kHz, 27 kHz at VLF) were included. Figure 2 summarizes the results of this second set of measurements.

The experimental results shown in Table 1 and Fig. 2 cover nearly 30 events over a period of several years and reveal a remarkably repeatable phenomenon. In every instance, the flares caused enhancement of noise in the ELF band (800 Hz and below) and the upper VLF band (21 kHz and 27 kHz). Conversely, in the lower VLF band the noise was decreased, with the decrease being much more severe at 5 kHz than 10 kHz. This decrease in noise gave rise to the term SDA (sudden decrease of atmospherics), with the overall effect of flares on background noise denoted by SEA/SDA. In several instances, the SEA/SDA effects were substantial, exceeding 10 dB in magnitude. The SEA/SDA effect at VLF had been noted by several authors (*Pierce, 1961; Chilton, et al., 1964; Crombie, 1965; Burgess and Jones, 1967*), but the SEA effects at ELF--which is of primary interest here--appears to have been measured solely by Sao and his collegues.

Table 1

MEASURED SEA/SDA RATIO IN DB

(A POSITIVE SIGN DENOTES AN SEA; A NEGATIVE, AN SDA)

(*Sao and Jindoh, 1966*)

Date	Frequency						
	30 Hz	100 Hz	260 Hz	600 Hz	10 kHz	21 kHz	27 kHz
2 May 1963	+1.7	+2.1	+5.9	+3.8	No observation	+1.0	+3.5
16 May 1963	+1.6	+2.0	+2.7	+2.9	-0.9	0	+1.5
20 May 1963	+1.0	+1.6	+1.9	+3.2	0	0	+1.0
21 May 1963	0	0	+2.5	-1.1	0	0	+3.0

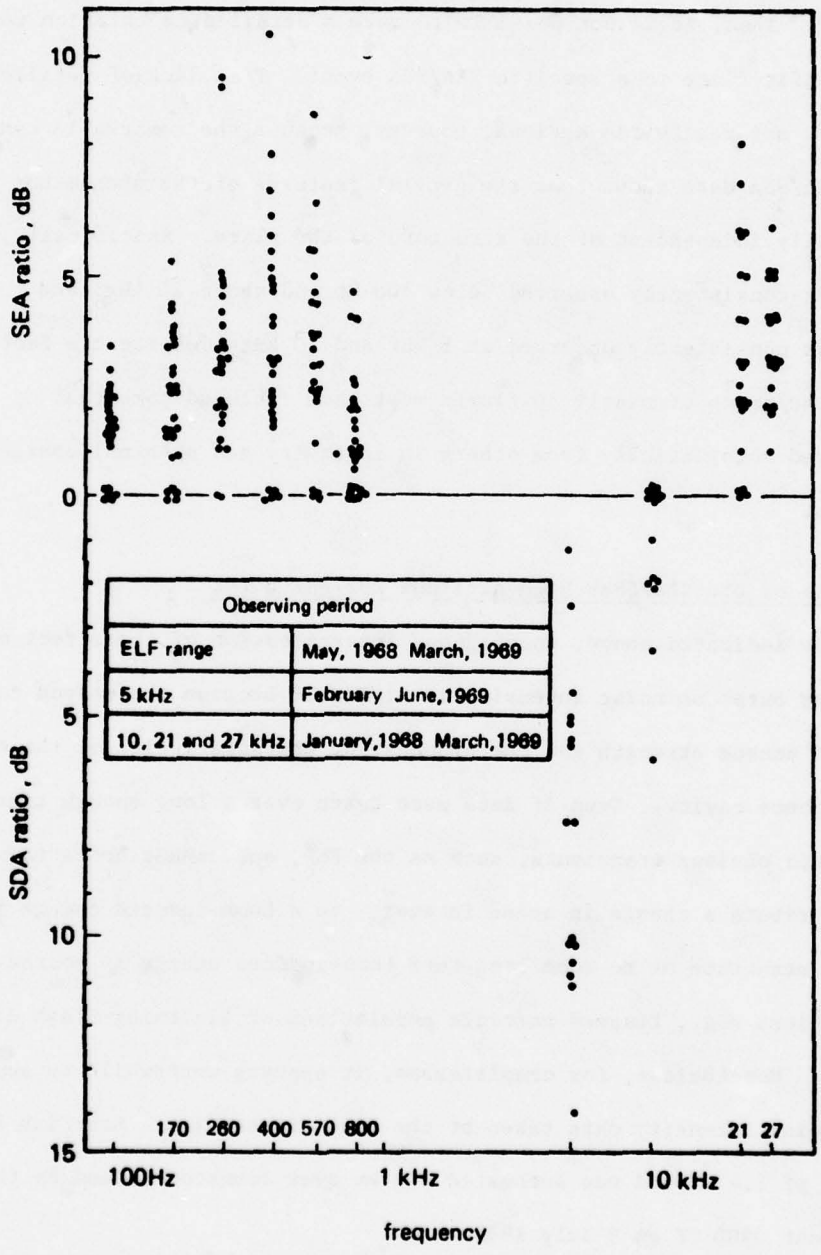

Fig. 2--Measured frequency spectrum of SDA/SEA (*Sao, et al., 1970*).

Unfortunately, no data are available on the intensity or spectrums of the incident x-rays responsible for the event shown in Table 1 or Fig. 2. Thus, it is not possible to make a detailed calculation relating a specific flare to a specific SEA/SDA event. This lack of detailed information is not really too serious, however, because the remarkable consistency of the SEA/SDA data shows that the general features of the phenomenon are virtually independent of the structure of the flare. Specifically, SEA was consistently observed below 800 Hz and above 20 kHz, and SDA was consistently observed at 5 kHz and 10 kHz--despite the fact that the group of nearly 30 flares must have included some that differed substantially from others in intensity and spectral characteristics.

Effects of the Starfish High-Altitude Nuclear Burst

As indicated above, unambiguous interpretation of the effect of a nuclear burst on noise intensity is difficult because the weapon can affect source strength and the propagation characteristics of the earth-ionosphere cavity. Even if data were taken over a long enough time period to avoid obvious transients, such as the EMP, one cannot be certain whether to attribute a change in noise intensity to a bomb-induced change in waveguide structure or to some long-term bomb-induced change in source characteristics; e.g., trapped-particle populations or lightning-flash distributions. Nonetheless, for completeness, it appears worthwhile to summarize ELF-noise intensity data taken at the time of Starfish. Starfish had a yield of 1.4 MT and was detonated 400 km over Johnston Island in the Pacific at about 0900 UT on 9 July 1962.

Teply, et al. (*1963*) measured the ELF background-noise intensity at frequencies between 5 Hz and 1.5 kHz at Tongatapu, which is about 3000-mi south of ground-zero. The data given in Table 2 were measured during time periods subsequent to the first few seconds after the burst and therefore avoid the transient EMP. In some instances, the nature of the data are such (e.g., sonograms or traces without scales) that only qualitative information can be given in Table 2.

Table 2

SUMMARY OF ELF DATA MEASURED AT TONGATAPU
BY TEPLY, ET AL. AT TIME OF STARFISH

Frequency Band	Behavior of Noise Intensity
5 Hz to 30 Hz	Around 6-dB enhancement persisting for at least 1 hr.
30 Hz to 60 Hz	No perciptible change during first hour.
60 Hz to 1500 Hz	Slight reduction; recovers in tens of minutes.

Effects of PCA Events

Larsen (*1974*) presents data--taken at Tromsø, Norway--on the behavior of ELF atmospheric noise during two PCA events. The first set of measurements--taken continuously during the 10-day period from 18 October 1969 to 6 November 1969--monitored frequency bands centered at 8 Hz, 35 Hz, 75 Hz, and 115 Hz. The measured field strength exhibited a 4-to-8 dB diurnal variation that qualitatively follows statistics for worldwide thunderstorm activity. A major PCA event started at around 1100 UT on 2 November 1969

and persisted for at least five days. Despite the strength and duration of this event, no significant change was noted in the intensity and temporal behavior of the noise at the four frequencies monitored.

Surprisingly, a small PCA that occurred on 24 January 1969 apparently caused a significant change in ELF noise intensity, whereas the major 2 November event discussed above did not. Figure 3 shows the measured power spectral density between a few hertz and 400 Hz before, during, and after the 24 January PCA. The PCA appears to have enhanced the noise somewhat at frequencies below about 100 Hz, and reduced the noise by several dB at frequencies between 100 Hz and 400 Hz. The difference in noise during the PCA (24 January) from that preceeding the PCA (20 January) cannot be attributed to diurnal variation of thunderstorm activity, because both measurements were taken at about the same time of day. However, Larsen states--and we agree--that the single set of measurements shown in Fig. 3 is inadequate to show conclusively that the 24 January PCA was the cause of the altered noise levels.

STRUCTURE OF SCHUMANN RESONANCES

Effects of the Starfish High-Altitude Nuclear Burst

The spectrums of electromagnetic background noise in the 5-to-30-Hz band were measured at the time of the Starfish high-altitude nuclear burst by Balser and Wagner (*1963*), Gendrin and Stefant (*1962*, *1964*), and Teply et al. (*1963*). By comparing the locations, f_n, of the spectral peaks before and after the burst, the shift, Δf_n, in each peak caused by the burst can be estimated.

The main results of these measurements are summarized in Table 3. The time constants of the measuring equipment varied from tens of seconds

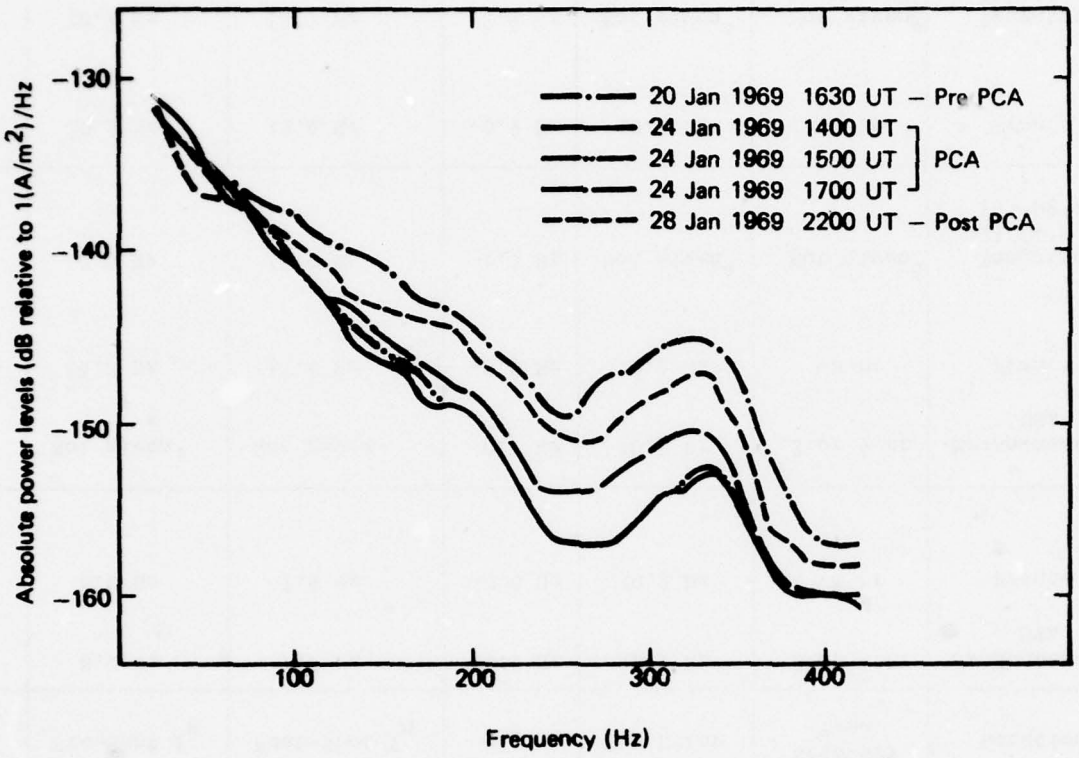

Fig. 3--Power spectral density function recorded at Lavangsdulen, Norway in 1969 (*Larsen, 1974*).

Table 3

SUMMARY OF MEASURED SHIFTS IN SCHUMANN-RESONANCE FREQUENCIES CAUSED BY THE STARFISH BURST

Resonance Number, n	Pre-Shot f_n	Post-Shot f_n	Δf_n	Exp. Error	Recovery Time	Location	Reference
1	8.2 Hz	7.7 Hz	-0.5 Hz	±0.1 Hz	3 or 4 hr	Massachusetts, USA	Balser and Wagner (1963)
1	8.0 Hz	7.4 Hz	-0.6 Hz	±0.2 Hz	∿8 hr	France	Gendrin and Stefant (1962, 1964)
2	Not given	Not given	-0.7 Hz	±0.1 Hz	3 or 4 hr	Massachusetts, USA	Balser and Wagner (1963)
2	14.2 Hz	13.6 Hz	-0.6 Hz	±0.2 Hz	∿8 hr	France	Gendrin and Stefant (1962, 1964)
2	14.5 Hz	13.0 Hz	-1.5 Hz	Not given[a]	Not given[a]	Tongatapu 21°14'S 175°08'W	Teply, et al. (1963)
3	20.3 Hz	19.4 Hz	-0.9 Hz	±0.2 Hz	∿8 hr	France	Gendrin and Stefant (1962, 1964)
3	20.7 Hz	18.3 Hz	-2.4 Hz	Not given[a]	Not given[a]	Tongatapu 21°14'S 175°08'W	Teply, et al. (1963)

(continued)

Table 3 (continued)

SUMMARY OF MEASURED SHIFTS IN SCHUMANN RESONANCE FREQUENCIES CAUSED BY THE STARFISH BURST

Resonance Number, n	Pre-Shot f_n	Post-Shot f_n	Δf_n	Exp. Error	Recovery Time	Location	Reference
4	26.5 Hz	25.6 Hz	-0.9 Hz	±0.4 Hz	∿8 Hr	France	Gendrin and Stefant (1962, 1964)
4	26.9 Hz	25.8 Hz	-1.1 Hz	Not given[a]	Not given[a]	Tongatapu	Teply, et. al (1963)

[a]Authors state that determination of spectral peak was "crude."

to several minutes; and, to within these timing uncertainties, the indicated changes in the resonant frequencies appeared to occur instantly. Teply, et al. did not specify uncertainties in their measured values of f_n, but stated that their determination of f_n subsequent to the shot was "very crude" because of smearing at the resonant peaks. Note that the measurements were made at three very widely spaced locations; viz., Tongatapu, about 3000-mi south of the burst; Massachusetts, about 6000-mi northeast of the burst; France, more than 8000 mi from the burst via a transpolar great-circle path.

The data consistently show that the Starfish burst caused the first few resonant frequencies to diminish by significant amounts. The magnitudes of the decreases depend on the resonance number, being about 1/2 Hz for the lowest resonance and around 1 Hz for the fourth resonance. The 2.4-Hz decrease in the third resonant frequency, f_3, reported by Teply, et al. is much larger than any of the other reported frequency shifts. In view of Teply's own statements regarding the imprecision of his spectral-peak determination, we treat his measurement of Δf_3 as spurious.

Unfortunately, no specific measurements were reported on the effect of Starfish on the Q's of the Schumann resonances. Visual inspection of spectrums presented by Teply, et al., however, shows that the spectral peaks were slightly smeared by the burst.* Also, the fifth and sixth resonances, which were visible on the pre-shot spectrums, were essentially undefined on the post-shot spectrums. Moreover, Balser and Wagner (*1963*) comment that the burst noticeably degraded the quality of the first few resonant peaks. Thus, although no quantitative conclusions can be drawn regarding Q, we feel justified in drawing the qualitative conclusion that Starfish caused the Qs to decrease somewhat.

---

*Our visual interpretation of these spectrums is not consistent with that of Teply, et al., who state that the burst produced "no noticeable change in the Q of the earth-ionosphere cavity."

Gendrin and Stefant (*1964*) present maps showing the locations of thunderstorm activity during the months of July. Statistically, the sources contributing to natural background electromagnetic noise at the time of Starfish would be expected to be heavily concentrated in Southeast Asia. Of course, the possibility exists that the Starfish burst altered the geographic distribution of noise sources.

Effects of PCA Events

Nelson (*1967*) presents data for the frequency and Q of the lowest Schumann resonance during three PCA events. The measured changes in f_1 and Q_1 are given in Table 4, along with the dates and times of the three events. This table also shows the nominal centers of the thunderstorm activity causing the atmospheric noise at the time of the PCA events. As would be expected, the PCA-induced changes are very similar to those described above for the Starfish burst. Specifically, the resonant frequency decreased by several tenths of a hertz and Q decreased by an ill-defined--but noticeable--amount.

Table 4

PCA-INDUCED CHANGES IN FREQUENCY AND Q OF LOWEST SCHUMANN RESONANCE; MEASURED IN MASSACHUSETTS

(*Nelson, 1967*)

f_1(Pre-PCA)	f_1(PCA)	Δf_1	ΔQ	Date	Local Standard Time	Thunderstorm Center
Not given	Not given	-0.2 Hz	"slight decrease"	6 July 1966	2030	Scattered
8.4 Hz	8.0 Hz	-0.4 Hz	"moderate increase"	28 Jan 1967	1000	Africa
8.2 Hz	7.4 Hz	-0.8 Hz	"slight decrease"	21 Feb 1967	1400	South America

Effects Of X-Ray Flares

A large number of measurements have been made by scientists from Japan during SIDs (*Sao, et al., 1971, 1973; Ogawa, et al., 1966; Ogawa and Tamaka, 1970*). Specifically, the correlations of the frequencies and Qs of the resonances with sunspot number, 1A-to-8A x-ray intensity, and magnetic Ap-index were determined. For the most part, these correlations are inconclusive, although an imaginative reader might discern an inverse relationship between 1) resonant frequency and sunspot number and 2) Q and Ap-index. Nelson (*1967*) gives data for the frequency and Q of the lowest resonance during a number of SIDs and concludes that individual events fail to produce discernible effects.

IV. COMPARISON BETWEEN CODE PREDICTIONS AND AVAILABLE DATA

This section compares the results of theoretical calculations with the experimental data described in Sec. III. The calculations are performed using Pacific-Sierra Research's full-wave propagation code (see, e.g., *Field, 1969; Field, 1970; Field, Lewinstein, and Dore, 1976*), which is virtually identical with ELF predictive codes developed and exercised under DNA auspices (see, e.g., *Pappert and Moler, 1970*). For ease of comparison, the various categories of data are discussed below in the same order as in Sec. III. This ordering, however, does not indicate the relative importance of the data categories. The data on the effects of x-ray flares on ELF noise intensity, and on the effects of the Starfish burst and PCA events on Schumann-resonance structure, are the most conclusive and strongly confirm key predictions of the propagation codes. On the other hand, data on the effects of Starfish and PCAs on ELF noise intensity, and on the effects of flares on Schumann resonances tend to be inconclusive, and neither strongly support nor strongly disagree with code predictions.

NOISE INTENSITY

Effects of X-Ray Flares

To compare code predictions with the experimental results given in Sec. III, calculations of ELF/VLF attenuation rate, phase velocity, and excitation factor are made for model ionospheres based on ambient conditions and a number of assumed solar-flare conditions. The ambient daytime model ionosphere is taken from the *DNA Blackout Handbook (Knapp and Schwartz, 1975)*; the disturbed ionospheres are calculated from assumed x-ray flares and spectrums using lumped-parameter de-ionoization equations and reaction rates also given in the *Blackout Handbook*. An infinite ground conductivity,

corresponding approximately to a sea water path, is assumed. Emphasis is placed on calculating flare-induced *changes* in propagation parameters rather than on absolute values, because the data given in Table 1 (p. 20) and Fig. 2 (p. 21) denote flare-induced changes in field strength.

The SEA and SDA indicate that the frequency dependence of flare-induced changes in ELF/VLF noise intensity is not sensitive to the detailed structure of a given flare. Moreover, these data are not presented in a form that permits direct comparison between a specific flare and a specific set of noise measurements. It is therefore not worthwhile to use detailed models of specific flares to make calculations. The most profitable approach is to perform calculations for a number of nominal--but realistic--flare models, and compare the ensemble of results thus obtained with the ensemble of data given in, e.g., Fig. 2.

It is not altogether unfortunate that the available data must be subjected to a pseudostatistical--rather than one-for-one--interpretation, because well-defined models of flares do not exist. The x-ray flux and spectrum is different for different flares, and changes during a given flare. Specifically, the flux tends to increase and the spectrum tends to harden as a flare progresses. X-rays in the 1-to-8-Å spectral band are most effective in influencing long-wave propagation, because they cause ionization in the D and lower E regions. Papers by De Jager (*1964, 1965*), Friedman (*1963*), Pounds (*1965*), and Van Allen (*1969*), among others, summarize data on x-ray flux and spectrum in this band. Integrated fluxes between 1Å and 8Å varying from hundredths to tenths of an erg/cm^2-sec were measured. A wide variety of spectra were noted, including sharp peaks in the 5-to-10-Å range, and quasi-thermal spectra at blackbody temperatures up to around 10^7K.

To represent the above conditions in the 1-to-8-Å band, we have performed calculations for several flare models having assumed integrated fluxes ranging from 0.05 erg/cm^2-sec to 0.2 erg/cm^2-sec, and characterized by both monoenergetic and blackbody spectra. The monoenergetic spectra were characterized by x-ray energy peaks between 1.5 KeV (8Å) and 3 KeV (4Å), and the blackbody spectra by "temperatures" between 5×10^6°K and 10^7°K.

Figure 4 shows the attenuation rate in decibels per megameter of propagation calculated for the ambient daytime model ionosphere, and ionospheres corresponding to model flares described above. Only the envelope of calculated values for the flare models is shown, because, as discussed above, comparison of the data with specific flares is not possible. The results given in Fig. 4 show that the attenuation rates calculated for the model flares are about equal to ambient below 100 Hz, lower than ambient between 100 Hz to 1 kHz, and between 10 kHz to 30 kHz, and higher than ambient between 5 kHz and 10 kHz. Since increased attenuation corresponds to signal degradation, the results in Fig. 4 are consistent with the SEA/SDA data in Table 1 and Fig. 2.

To better illustrate the agreement between calculations and experiment, the results from Fig. 4 have been plotted in a different format in Fig. 5, which shows the *difference* between attenuation rates calculated for the model flares and those calculated for the model ambient ionosphere. The sign of this difference has been reversed to account for the fact that an increase in attenuation rate corresponds to a decrease in electromagentic field intensity. Thus, Fig. 5 shows the flare-induced enhancement or degradation per megameter of propagation path exposed to the flare.

In addition to enhancements or degradations that are due to propagation and are proportional to exposed pathlength, solar flares can affect the

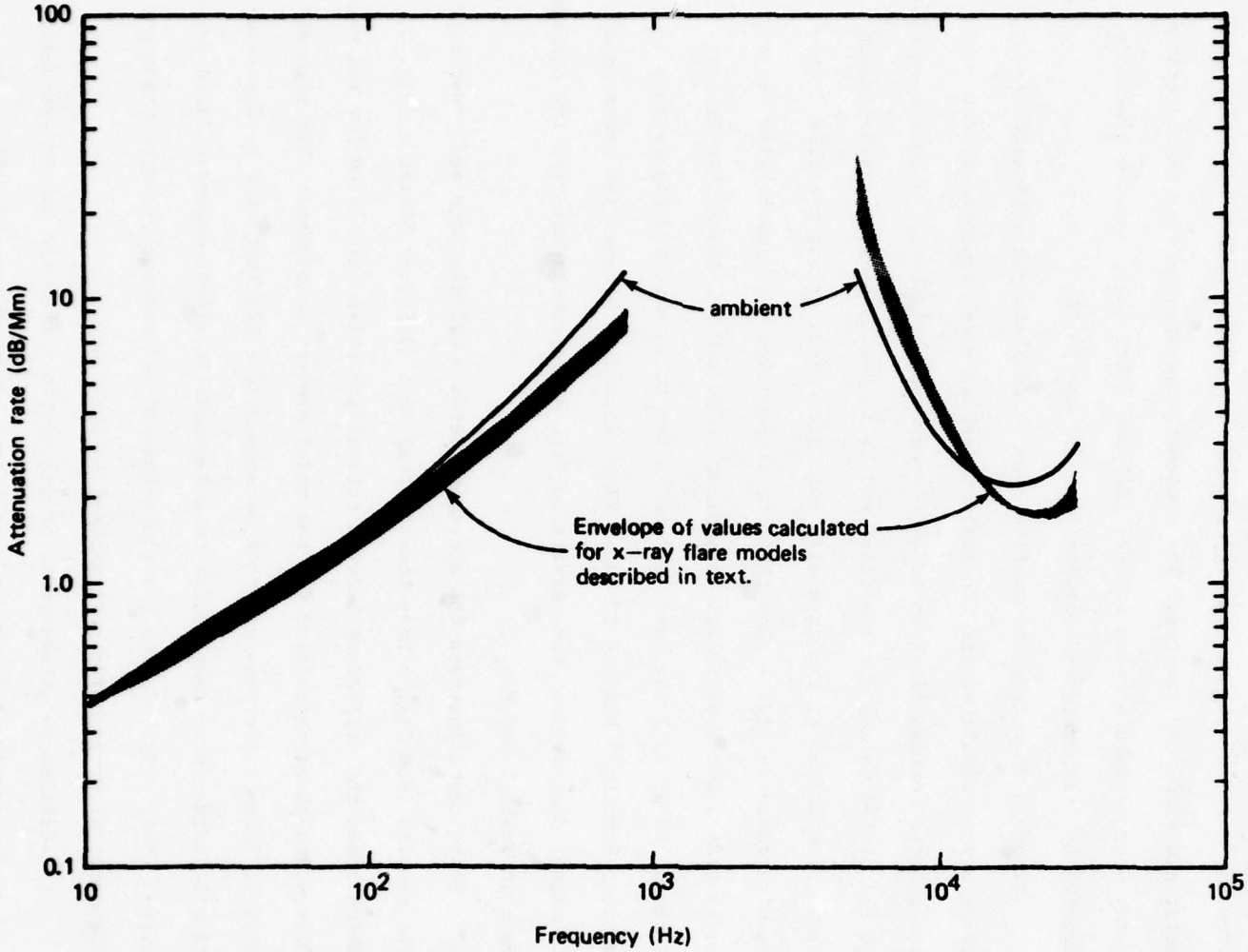

Fig. 4--Calculated ELF/VLF attenuation rates for daytime ambient conditions and several model solar-flare environments.

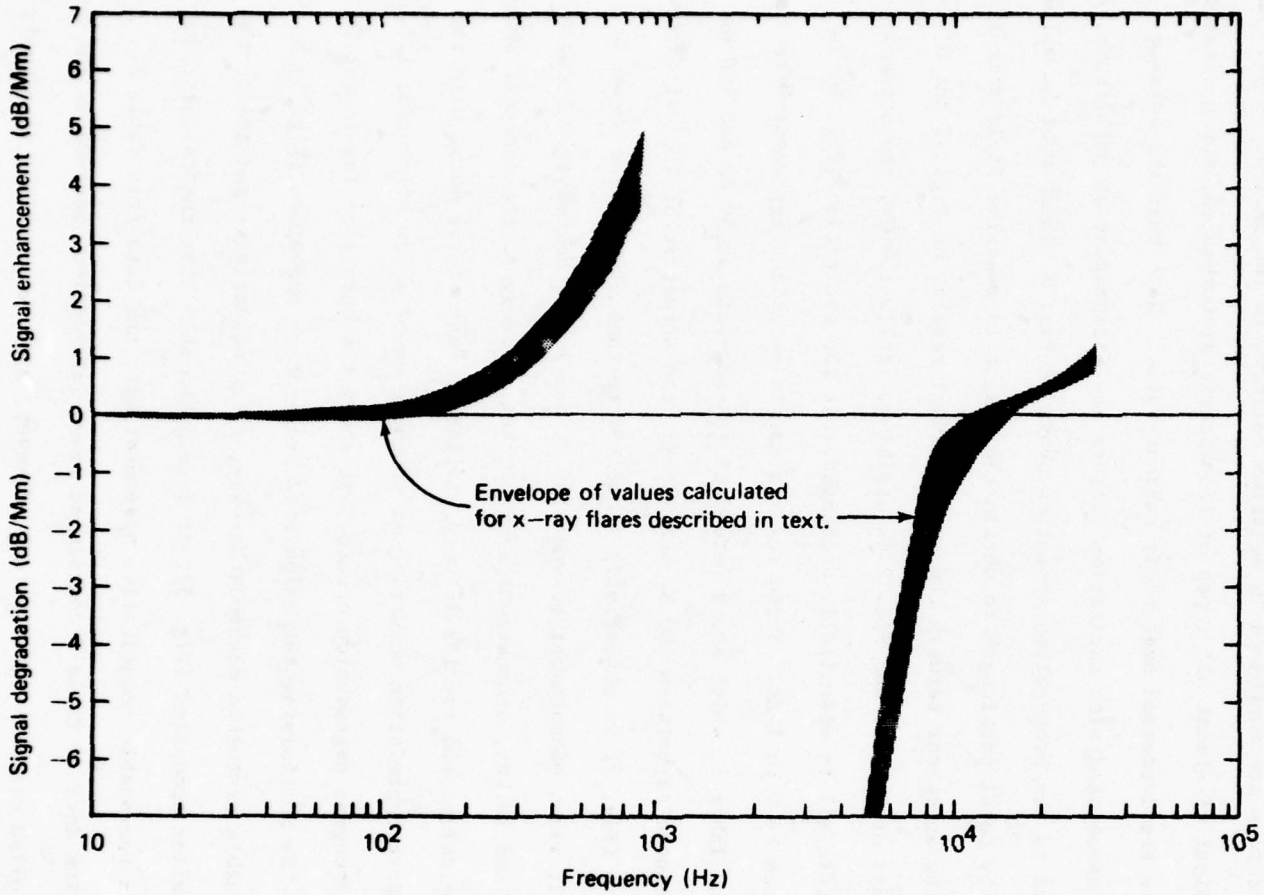

Fig. 5--Calculated changes in ELF/VLF attenuation rate relative to ambient for several model solar-flare environments

excitation factor of the dominant waveguide modes. Figure 6 shows the calculated excitation factors for the model solar flares. These excitation factors are expressed in decibles relative to the ambient value. As is typical of almost all types of ionospheric disturbances, the excitation factors are increased over their ambient value. Note that the enhancements associated with excitation factors are independent of pathlength, as opposed to the propagation anomalies shown in Fig. 5, which must be multiplied by total pathlength to obtain the change in measured field strength.

The agreement between the computational results of Figs. 5 and 6 with the data of Table 1 and Fig. 2 is striking. Below 100 Hz, the attenuation rate (Fig. 5) is essentially unchanged, but the excitation (Fig. 6) is enhanced by 0 to 1 dB. These results are in excellent agreement with the data of Table 1, which shows 0-to-2 dB enhancements at 30 Hz and 100 Hz. At frequencies between 100 Hz and 30 kHz, the structure of the calculated results (Fig. 5) is essentially identical to that of the data shown in Fig. 2; viz., enhancement between 100 Hz and 1 kHz, degradation between 5 kHz and 10 kHz, enhancement above 10 kHz. Moreover, the spectral shape of the calculated results is very similar to that of the data, with the strongest degradation occurring at frequencies of a few kilohertz; i.e., the strongest degradation occurs just above the cutoff of the lowest TM mode. By multiplying the calculated propagation anomalies (Fig. 5) by reasonable disturbed pathlengths--say, a few megameters--and adding the excitation anomalies (Fig. 5), it is easy to show that the calculations are in reasonable quantitative agreement with the data from Table 2.

The data of Table 2 contain no phase information, because of the non-controlled nature of the source. However, many observations of signals

For the above reason, the best that can be done is to give a tentative qualitative explanation of the data. Table 2 shows that subsequent to Starfish the noise intensity increased at frequencies below about 30 Hz and was essentially unchanged at higher frequencies. Many existing ELF calculations (e.g., *Field, 1969*) show that the effect of a large disturbance such as a nuclear burst or strong PCA is to increase both the excitation factor and attenuation rate. The increase in excitation is relatively constant--typically several dB--over the entire band, whereas the increase in attenuation rate becomes more severe as the ELF frequency is increased. The result is the well-known competition at ELF between improved excitation and degraded propagation (increased attenuation) that can give either a net increase or decrease in measured field strength. Qualitatively, the improved excitation would be expected to dominate the degraded propagation at the lower ELF frequencies, and to become less important relative to the degraded propagation at the higher frequencies. This general behavior is consistent with the data given in Table 2.

Effects of PCA Events

As indicated in Sec. III, the available data on the effects of PCA events on ELF noise intensity are inadequate for quantitative interpretation. The net effect of an ionospheric disturbance on ELF noise intensity depends strongly on the location and orientation of the propagation path relative to the disturbed region. Neither the geographic extent of the PCA nor the location of the noise sources relevant to the data in Fig. 3 are known with any precision. Thus, it is not possible to calculate the net effect of the above-mentioned competition between improved excitation and degraded propagation. Although surprising at first glance, the fact

that a small PCA apparently caused a greater change in noise strength than did a large event is not necessarily at variance with code predictions. The large PCA simply could have caused an increase in excitation that compensated for a degradation in propagation. Thus, we conclude that these data are inconclusive.

STRUCTURE OF SCHUMANN RESONANCES

Effects of the Starfish High-Altitude Burst

We use Eqs. (19) and (20) to compare theoretical predictions of the peak frequencies, f_n, and Q's of the Schumann resonances with data given in Sec. III. Empahsis is placed on bomb-induced shifts, Δf_n, in peak frequencies shown in Table 3 (pp. 20-21) because the main goal of propagation codes is to predict signal changes caused by changes in ionospheric structure. Interpretation of Schumann-resonance data is quite unambiguous because the structure of the resonances depends mainly on the state of the ionosphere, being independent of source strength.

To use Eq. (19), we need theoretical calculations of the characteristic change, ΔS_R, in relative phase velocity caused by the Starfish burst. In addition, we need an estimate of the fraction, F, of the earth's circumference--drawn through source and receiver--that is subjected to levels of disturbance characterized by ΔS_R. As discussed in Sec. II, ΔS_R exhibited strong geographic disturbance after Starfish, and a well-defined value does not exist. Moreover, although the main sources of atmospheric noise at the time of Starfish were probably centered somewhere in Southeast Asia, an accurate source location is not known. These facts, coupled with the diffuse boundaries of the bomb-disturbed region, make an accurate value of the fraction, F, impossible. Thus, the best that can be hoped for is semiquantitative agreement between code predictions and available data.

The first step in estimating ΔS_R is to determine the value of S_R that obtained prior to the burst. Even this step is imprecise because the

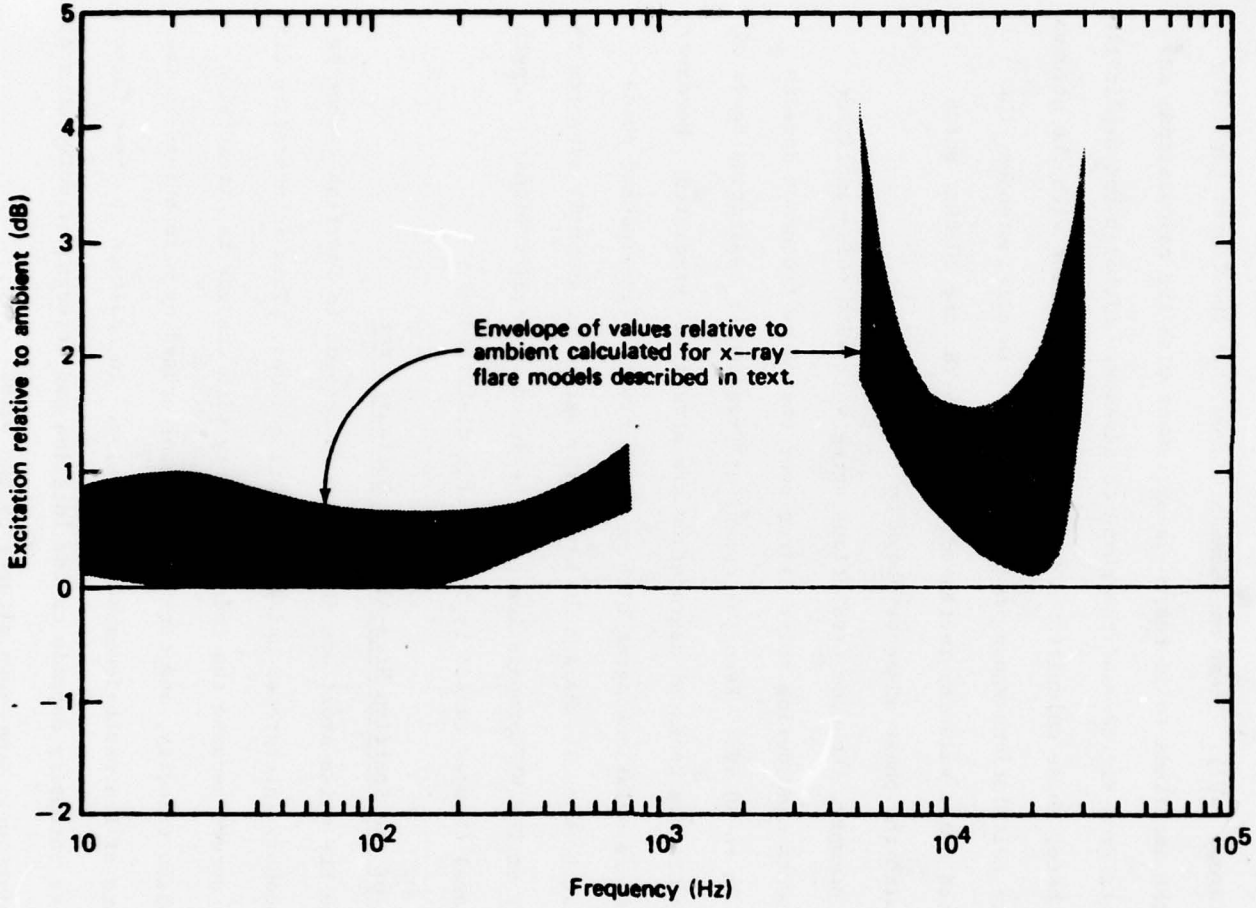

Fig. 6--Calculated changes in ELF/VLF excitation factor relative to ambient for several model solar-flare environments

from VLF transmitters in the 16-to-20 kHz range have been made during flares (e.g., *Crombie, 1965; Chilton, et al., 1964; Burgess and Jones, 1967; Pierce, 1961*). These measurements show that the flares generally caused the amplitude to increase--in agreement with the calculations and noise data from Fig. 2--and the phase to advance. Although not explicitly plotted here, phase calculations were made in conjunction with the attenuation rate calculations shown in Figs. 4 and 5. In all instances, the calculated phase velocity increased between 16 kHz and 20 kHz, which agrees with the phase advances shown by the data.

In summary, the code predictions agree well with noise-amplitude measurements made during solar flares over the three frequency decades from 30 Hz to 30 kHz. Even the crossover frequencies separating bands of enhancement from bands of degradation are accurately predicted. Moreover, VLF phase calculations agree with measurements of flare-induced phase anomalies between 16 kHz and 20 kHz. This agreement strongly supports the validity of ELF/VLF propagation codes designed to predict signal strength (and phase) changes caused by ionospheric disturbances.

Effects of the Starfish High-Altitude Nuclear Burst

The ELF noise-amplitude data taken subsequent to Starfish cannot be unambiguously interpreted using propagation codes. This interpretive difficulty occurs because the codes deal only with changes in attenuation rate, phase velocity, and excitation factor caused by alterations in the structure of the earth-ionosphere waveguide. In addition to these factors, the noise intensity depends on the location and strength of noise sources, which might well have been altered by the burst.

propagation paths pertinent to Schumann resonances completely encircle the earth, and some averaging between day and night conditions is needed. Moreover, on the nighttime portion of the path, S_R depends on propagation direction. The average ambient values used for S_R taken from Galejs (*1972*) are as follows: 1.35 at 8 Hz (f_1), 1.3 at 14 Hz (f_2), 1.27 at 20 Hz (f_3), and 1.25 at 26.5 Hz (f_4).

The full-wave propagation code is used to calculate values of S_R subsequent to the Starfish burst. These calculated values depend on distance from the burst, and a single value cannot be given. Fortunately, once a relatively strong level of ionospheric disturbance has been reached, the impact on ELF propagation tends to be saturate; and further increases in the level of disturbance cause relatively small changes in ELF propagation parameters. Thus, it is possible to define values of S_R that correspond roughly to a fairly wide range of strongly disturbed conditions. By performing a number of numerical calculations for nuclear environments of various intensities, we find the following values to reasonably characterize S_R in strongly disturbed regions: 1.7 at 8 Hz (f_1); 1.6 at 14 Hz (f_2); 1.5 at 20 Hz (f_3); 1.45 at 26.5 Hz.

By inserting the above disturbed and undisturbed values for S_R in Eq. (19), it is easily shown that the theoretically predicted Starfish-induced shifts in resonant frequencies become

$$\Delta f_n \begin{cases} \sim -2F \text{ Hz} & \text{for } f_1 (8 \text{ Hz}) \\ \sim -3F \text{ Hz} & \text{for } f_2 (14 \text{ Hz}) \\ \sim -3.5F \text{ Hz} & \text{for } f_3 (20 \text{ Hz}) \\ \sim -4F \text{ Hz} & \text{for } f_4 (26.5 \text{ Hz}) \end{cases} . \tag{21}$$

Again, recall that F is the fraction of the appropriate round-the-world propagation path significantly affected by the weapon. Note that Starfish

affected enormous regions due to line-of-sight radiation from the burst and subsequent far-flung debris, conjugate zone affects, and neutron-decay β particles impinging on the ionosphere well beyond line-of-sight. Thus, although it is impossible to accurately determine F, values in the range of 0.15 to 0.3 seem reasonable for so widespread a disturbance as Starfish. The larger values in this range apply to Teply's Tongatapu Station, which was squarely in the conjugate zone. Insertion of these values for F into Eq. (21) gives good semiquantitative agreement with the data in Table 2 (p. 23). Specifically, the codes correctly predict that 1) the Starfish burst should have caused downward shifts in the Schumann resonance frequencies, 2) that the magnitude of these downward shifts is between several tenths of a hertz and around a hertz,* and 3) the greatest frequency shifts occur for the higher order resonances.

The same numerical calculations used to obtain the values of S_R given above show that a strong disturbance such as Starfish will cause the attenuation rate, β, to increase by a few tens of percent at 8 Hz and by up to a factor of two at 26.5 Hz. Insertion of these values for $\Delta\beta/\beta$ into Eq. (20) show that the codes predict a decrease in the Q's of the resonances, with the greatest predicted decreases occuring for the higher-order resonances. This result is consistent with the qualitative data interpretation given in Sec. III; viz., Starfish apparently caused the Q's to decrease "somewhat." Absence of better data on the behavior of the Q's makes more quantitative conclusions regarding agreement between experiment and theory impossible. As pointed out in the derivation given in Sec. II, however, the fact that the codes correctly predict ΔS_R virtually guarantees the correctness of predicted changes in attenuation rate.

---

*Recall that Teply's measurement of -2.4 Hz for Δf_3 is probably spurious.

Effects of PCA Events

Table 2 (p. 23) summarizes the data on the effects of PCA events on the lowest Schumann resonance. Of the three events shown, only those of 28 January and 21 February 1967 are considered here. The 6 July event is difficult to interpret because only partial data are available and, because of the time of the event, no reasonable assumptions can be made regarding the location of major thunderstorm centers. No information was given on the structure of the PCAs or the ionosphere at the time of the measurements summarized in Table 2. Thus, as was the situation for the ELF noise measurements taken during flares, there is no point in attempting detailed correlations between specific flares and the measured values of $\Delta\beta_1$ and ΔQ. Again, the best that can be done is to compare the data with calculations based on several nominal PCA models.

Table 5 summarizes the results of calculations based on three nominal PCA-disturbed daytime ionospheres designated generically as strong, moderate, and weak. All models are based on actual events, albeit not the ones of 28 January and 21 February 1967, and are similar to those discussed by Field *(1970)*. The calculations are performed for a frequency of 8 Hz, which corresponds closely to the center frequency of the lowest Schumann resonance. As has been done throughout this report, we concentrate on the changes, ΔS_R and $\Delta\beta$, produced by the disturbance rather than on the absolute values of S_R and β. In Table 5, ΔS_R and $\Delta\beta$ denote the difference between the disturbed and the ambient values. Table 5 also includes nominal ambient values for S_R and β, averaged over daytime and nighttime conditions.

As was the situation for interpreting the Starfish data, it is necessary to estimate the factor F before applying Eqs. (19) and (20). For the

Table 5

CALCULATED PROPAGATION PARAMETERS FOR SEVERAL MODEL IONOSPHERES AND f = 8 Hz

	$S_R = c/v$	ΔS_R	β(dB/Mm)	$\Delta\beta$(dB/Mm)
Strong PCA	1.7	0.35	0.37	0.12
Moderate PCA	1.7	0.35	0.40	0.15
Weak PCA	1.55	0.20	0.34	0.11
Average ambient (*Galejs, 1972*)	1.35	--	0.25	--

21 February event, the main thunderstorm centers were probably in South America, and the great-circle path connecting this source location to the receiver location in Massachusetts is essentially in the North-South direction. Thus, the round-the-world path containing source and receiver passes squarely through both polar caps, and--depending, of course, on the details of the particular PCA--nearly one-third of this path can be assumed covered by the disturbance. Thus, we use $F \approx 0.3$ for the 21 February PCA event.

Inserting $F = 0.3$ and $\Delta S_R/S_R$ from Table 5 into Eq. (19) gives $\Delta f_1 \sim -0.6$ Hz for moderate-to-strong PCAs and $\Delta f_1 \sim -0.35$ Hz for weak PCAs. Given the many uncertainties in the calculation, the agreement between these results and the experimental value of $\Delta f_1 = -0.8$ Hz is satisfactory. Inserting $F = 0.3$ and $\Delta\beta/\beta$ from Table 5 into Eq. (20) indicates that the 21 February PCA would have been expected to decrease Q_1 by between 15 percent and 20 percent. These predictions are in qualitative agreement with the observed "slight decrease" indicated in Table 2.

At the time of the 28 January 1967 PCA, the most likely location of the important thunderstorm centers was in Africa. The round-the-world path connecting Africa and Massachusetts passes close to the extremities of the polar caps rather than squarely through them. Therefore, contrary to the 21 February PCA discussed above, the full impact of the 28 January PCA was probably not reflected in the Massachusetts measurement. Roughly half of the first Fresnel zone of the propagation path followed by the atmospheric noise would be subjected to the PCA-disturbed ionosphere. Field (*1978*) showed that, in such a circumstance, the effect of the PCA would be about half that obtained if the entire Fresnel zone had been affected. Thus, whereas the 21 February event was calculated to have caused a shift, Δf_1,

of between -0.35 Hz and -0.6 Hz--depending on the strength of the event--the corresponding numbers for the 28 January event would be between -0.18 Hz and -0.3 Hz. Again, given the many uncertainties, these results agree tolerably well with the measured value (Table 2) of $\Delta f_1 \approx -0.4$ Hz.

The fact that the data indicates a "moderate" decrease in Q_1 on 28 January versus only a "slight" decrease for the apparently more potent 21 February event is somewhat puzzling, although not too significant in view of the qualitative nature of the data on Q_1.

Effects of X-Ray Flares

Data briefly summarized in Sec. III show minimal correlation between SIDs and the frequencies and Q's of Schumann resonances. Calculations using the solar-flare model ionospheres discussed above give very slight differences between ambient and disturbed values of S_R and β at Schumann-resonance frequencies. Thus, in a trivial sense, the calculations and data are consistent. No significant effects were calculated and none were observed.

V. CONCLUSIONS

An extensive literature survey has identified a number of low-frequency noise measurements relevant to the effects of ionospheric disturbances on ELF propagation. These measurements pertain to the behavior of earth-ionosphere cavity resonances and ELF/VLF noise intensity at the time of 1) the Starfish high-altitude nuclear detonation, 2) more than thirty solar flares, and 3) two polar-cap-absorption events (PCAs). Until controlled-source ELF experiments are carried out under disturbed conditions, these collateral data provide the only means by which codes that predict ELF propagation anomalies in nuclear environments can be compared with experiment.

A full-wave propagation code similar to predictive codes developed under DNA auspices has been used above to compute ELF propagation anomalies due to Starfish, PCA events, and a large number of model x-ray flares. The results of these calculations are compared--to the extent possible--to the available data. Despite the inadequacies of the data, we are able to verify key theoretical predictions.

Good agreement is demonstrated between code predictions and ELF/VLF noise intensity during solar flares. Both experiment and theory consistently show that the vast majority of flares cause the intensity to increase at frequencies between 30 Hz and 1 kHz, decrease between 5 kHz and 10 kHz, and increase between 10 kHz and 30 kHz. This agreement, which occurs over three frequency decades, strongly implies the correctness of the predictive codes.

Although the Schumann-resonance band (8-to-30 Hz) is somewhat lower than the ELF communications band (45-to-80 Hz), both bands propagate in the

TEM waveguide mode. Data on Schumann resonances may therefore be meaningfully compared with the outputs of ELF propagation codes. The results of such a comparison made in this report semiquantitatively support the validity of the codes. Specifically, the numerical calculations correctly predict that either Starfish or the PCAs would cause the peak frequencies of the Schumann resonances to shift downward by 0.5 Hz to 1 Hz and the Q's of the resonances to decrease. The shift in resonant frequencies is due to the depressed ionosphere causing the phase velocity of the signal to decrease, and the decrease in Q is caused by an increase in the attenuation rate in the earth-ionosphere waveguide.

REFERENCES

1. Balser, M., and C. A. Wagner, "Observations of Earth-Ionosphere Cavity Resonances," *Nature*, 188, 1960, pp. 638-641.

2. -----, "Effect of a High-Altitude Nuclear Detonation on the Earth-Ionosphere Cavity," *Journ. Geophys. Res., Vol. 68*, No. 13, 1 July 1963, pp. 4115-4118.

3. Budden, K. G., *The Waveguide Mode Theory of Wave Propagation*, Logos Press, London, 1961.

4. Burgess, B., and T. B. Jones, "Solar Flare Effects and VLF Radio Wave Observations of the Lower Ionosphere," *Radio Science*, 2(6), 1967, pp. 619-626.

5. Chilton, C. J., F. K. Steele, and D. D. Crombie, "An Atlas of Solar Flare Effects Observed on Long VLF Paths During 1961," *NBS Technical Note 210*, March 1964.

6. Crombie, D. D., "On Use of VLF Measurements for Obtaining Information on Lower Ionosphere," *Proc. IEEE*, 53(12), 1965, pp. 2027-2034.

7. De Jager, C., "Solar Ultraviolet and X-ray Radiation," in *Research in Geophysics*, Chap. 1., M.I.T. Press, Cambridge, Mass., 1964.

8. -----, "Solar X Radiation," *Ann. Astrophys., 28*(1), 125-131, 1965.

9. Field, E. C., "Propagation of ELF Waves Under Normal or Naturally Disturbed Conditions," *Journ. Geophys. Res., 74*, 1969, pp. 3639-3650.

10. -----, "The Effects of Ions on Very-Low-Frequency Propagation During Polar-Cap-Absorption Events," *Radio Science*, Vol. 5, March 1970, pp. 591-600.

11. -----, *ELF Propagation in a Non-Stratified Earth-Ionosphere Waveguide*, Pacific-Sierra Research Corporation, Report 806, April 1978.

12. Field, E. C., M. Lewinstein, and M. A. Dore, *Effects of Antenna Elevation and Inclination on VLF/LF Signal Structure*, Pacific-Sierra Research Corporation, RADC-TR-76-C-375, December 1976.

13. Friedman, H., "Ultraviolet and X-rays from the Sun," *Ann. Rev. Astron. Astrophys.*, 1(59) 1963.

14. Galejs, J., *Terrestrial Propagation of Long Electromagnetic Waves*, Pergamon Press, New York, 1972.

15. Gendrin, R., and R. Stefant, "Effet de l'explosion thermonucléaire a' trés haute altitude du 9 julliet 1962 sur la résonance de la cavité terre-ionosphere. Resultats experimentaux." *Compte Rendus, Tome 255*, No. 18, 29 October 1962, Paris, pp. 2273-2275.

16. Gendrin, R., and R. Stefant, "Magnetic Records Between 0.2-30 c/s, Chapter 26 in *Propagation of Radio Waves at Frequencies Below 300 kc/s*, ed. W. T. Blockband, The MacMillan Co., New York, 1964.

17. Imhoff, W. L., et al., *Analysis of Satellite Data on Precipating Particles in Coordination with ELF Propagation Anomalies*, Lockheed Missile and Space Co., LMSC-D-502063, 30 April 1976.

18. Knapp, W. S., and K. Schwartz, "Aids for the Study of Electromagnetic Blackout," General Electric/TEMPO, DNA 3449, 1 February 1975.

19. Larsen, T., "ELF Noise Measurements," *ELF-VLF Radio Wave Propagation*, ed. J. A. Holtet, D. Reidel Publishing Co., Dodrecht-Holland, 1974, pp. 233-238.

20. Nelson, R., *Ionospheric Perturbation and Schumann Resonance Data*, Ph.D. Dissertation, Massachusetts Institute of Technology, Dept. of Geology and Geophysics, 12 May 1976.

21. Ogawa, T., et al., "ELF Noise-Bursts and Enhanced Oscillations Associated with the Solar-Flare of July 7, 1966," *Rep. Ionos. Space Res. Japan, Vol. 20*, 1966, pp. 528-536.

22. Ogawa, T., and Y. Tanaka, "Q Factors of the Schumann Resonances and Solar Activity," *Special Contributions, Geophysical Institute, Kyoto University*, No. 10, 1970, pp. 21-28.

23. Pappert, R. A., and W. F. Moler, "Propagation Theory and Calculations at Lower Extremely Low Frequencies (ELF)," *IEEE Trans. on Comm.*, Volume COM-22, April 1974, pp. 438-451.

24. Pierce, E. T., "Attenuation Coefficients for Propagation at Very Low Frequencies (VLF) During a Sudden Ionospheric Disturbance (SID)," *J. Res. NBS, Radio Propagat.*, 65D(6), November-December 1961, pp. 543-546.

25. Pounds, K. A., "Recent Solar X-ray Studies in the United Kingdom," *Ann. Astrophys.*, 28(I), 1965, pp. 132-145.

26. Sao, K., and H. Jindoh, "SEA Phenomenon on E.L.F. Atmospherics," *Journ. of Atmospheric and Terrestrial Physics, Vol. 28*, 1966, pp. 97-98.

27. Sao, K., et al., "Sudden Enhancements (SEA) and Decreases (SDA) of Atmospherics," *Journ. of Atmospheric and Terrestrial Physics*, Vol. 32, 1970, pp. 1567-1576.

28. -----, "Day to Day Variation of Schumann Resonance Frequency and Occurrence of Pc 1 in View of Solar Activity," *Jovrn. Geomagnetism and Geoelectricity*, Vol. 23, Nos. 3, 4, 1971, pp. 411-415.

29. -----, "Experimental Investigation on Schumann Resonance Frequencies," *Electronics and Communications in Japan*, Vol. 56-B, No. 6, 1973, pp. 80-85; and *Journ. of Atmospheric and Terrestrial Physics*, Vol. 35, 1973, pp. 2047-2053.

30. Teply, L., et al., *Sub ELF Geomagnetic Fluctuations, Vol. III, Observations of Transient and Background VLF, ELF, and Sub ELF Electromagnetic Effects Produced by High-Altitude Nuclear Detonations*, Lockheed Missiles & Space Company, Final Report AF 19(628)-462, 26 December 1963.

31. Van Allen, J. A., and C. D. Wende, "The Solar Flare of July 8, 1968," *J. Geophys. Res.*, 74(11), 3046, 1 June 1969.

DISTRIBUTION LIST

DEPARTMENT OF DEFENSE

Assistant Secretary of Defense
Comm, Cmd, Cont. & Intell.
ATTN: M. Epstein
ATTN: J. Babcock

Assistant to the Secretary of Defense
Atomic Energy
ATTN: Executive Assistant

Command & Control Technical Center
Department of Defense
ATTN: C-312, R. Mason
ATTN: C-650, G. Jones
ATTN: C-650, W. Heidig

Defense Advanced Rsch. Proj. Agency
ATTN: TIO

Defense Communications Engineer Center
ATTN: Code 720, J. Worhtington
ATTN: Code R410, J. McLean

Defense Communications Agency
ATTN: Code 810, J. Barna
ATTN: Code 480
ATTN: Code 101B
ATTN: Code R1033, M. Raffensperger

Defense Documentation Center
12 cy ATTN: DD

Defense Intelligence Agency
ATTN: DC-7D, W. Wittig
ATTN: DB-4C, E. O'Farrell
ATTN: HQ-TR, J. Stewart
ATTN: DB, A. Wise
ATTN: DT-5
ATTN: DT-1BZ, R. Morton
ATTN: DT-1B

Defense Nuclear Agency
ATTN: DDST
ATTN: STVL
3 cy ATTN: RAAE
4 cy ATTN: TITL

Field Command,
Defense Nuclear Agency
ATTN: FCPR

Interservice Nuclear Weapons School
ATTN: TTV

Joint Chiefs of Staff
ATTN: J-3, WWMCCS Evaluation Office

Joint Strat. Tgt. Planning Staff
ATTN: JPST, G. Goetz
ATTN: JLTW-2

Field Command
Defense Nuclear Agency
Livermore Division
ATTN: FCPRL

DEPARTMENT OF DEFENSE (Continued)

National Security Agency
Department of Defense
ATTN: R52, J. Skillman
ATTN: B3, F. Leonard
ATTN: W32, O. Bartlett

Under Secretary of Defense for Rsch. & Engrg.
ATTN: Strategic & Space Systems (OS)

WWMCCS System Engineering Org.
ATTN: R. Crawford

DEPARTMENT OF THE ARMY

Atmospheric Sciences Laboratory
U.S. Army Research & Development Command
ATTN: DELAS-AE-M, F. Niles

Electronics Tech. & Devices Lab.
U.S. Army Electronics R & D Command
ATTN: DELET-ER, H. Bomke

Harry Diamond Laboratories
Department of the Army
ATTN: DELHD-N-NP
ATTN: DELHD-N-RB, R. Williams
ATTN: DELHD-N-NP, F. Wimenitz
ATTN: DELHD-N-TI, M. Weiner

U.S. Army Ballistic Research Labs.
ATTN: Tech. Library

U. S. Army Comm-Elec. Engrg. Instal. Agency
ATTN: CCC-EMEO, W. Nair
ATTN: CCC-EMEO-PED, G. Lane

U.S. Army Foreign Science & Tech. Center
ATTN: DRXST-SD

U.S. Army Materiel Dev. & Readiness Command
ATTN: DRCLDC, J. Bender

U.S. Army Nuclear & Chemical Agency
ATTN: Library

U.S. Army TRADOC Systems Analysis Activity
ATTN: ATAA-PL
ATTN: ATAA-TCC, F. Payan, Jr.
ATTN: ATAA-TDC, J. Hesse

DEPARTMENT OF THE NAVY

Naval Electronic Systems Command
ATTN: NAVELEX 3101, T. Hughes
ATTN: PME 117
ATTN: Code 5011
ATTN: PME 117-T

Naval Intelligence Support Center
ATTN: NISC-50

Naval Ocean Systems Center
ATTN: Code 8151, C. Baggett
3 cy ATTN: Code 5324, W. Moler

DEPARTMENT OF THE NAVY (Continued)

Naval Research Laboratory
ATTN: Code 7580
ATTN: Code 7555
ATTN: Code 6700, T. Coffey
ATTN: Code 6707, J. Davis
ATTN: Code 7500, Hg. Comm. Dir., B. Wald
ATTN: Code 6701, J. Brown

Naval Surface Weapons Center
White Oak Laboratoy
ATTN: Code F31

Office of Naval Research
ATTN: Code 420
ATTN: Code 421

Office of the Chief of Naval Operations
ATTN: Op-604
ATTN: Op-941

Strategic Systems Project Office
Department of the Navy
ATTN: NSSP-2722, F. Wimberly
ATTN: NSP-2141

DEPARTMENT OF THE AIR FORCE

Aerospace Defense Command
Department of the Air Force
ATTN: DC, Mr. Long

Aerospace Defense Command
Department of the Air Force
ATTN: XPDQ
ATTN: XP

Air Force Geophysics Laboratory, AFSC
ATTN: LKB, K. Champion
ATTN: OPR1, J. Ulwick
ATTN: PHP, J. Aarons
ATTN: PHI, J. Buchau
ATTN: PHP, J. Mullen
ATTN: OPR, A. Stair

Air Force Weapons Laboratory
ATTN: DYC, J. Barry
ATTN: SUL
ATTN: DYC, J. Kamm

Deputy Chief of Staff
Research, Development, & Acq.
Department of the Air Force
ATTN: AFRDQ

Deputy Chief of Staff
Program and Analyses
Department of the Air Force
ATTN: PACSC, R. Paul

Electronic Systems Division, AFSC
ATTN: XRW, J. Deas
ATTN: YSEA

Foreign Technology Division, AFSC
ATTN: TQTD, B. Ballard
ATTN: NIIS, Library

Rome Air Development Center, AFSC
ATTN: EEP

DEPARTMENT OF THE AIR FORCE (Continued)

Air Logistics Command
Department of the Air Force
ATTN: MM, R. Blackburn

Space & Missile Systems Organization
Air Force Systems Command
ATTN: MNNL, S. Kennedy

Strategic Air Command
Department of the Air Force
ATTN: NRT
ATTN: DCX

DEPARTMENT OF ENERGY

Department of Energy
ATTN: Office of Military Application (RD&T)

OTHER GOVERNMENT AGENCIES

Central Intelligence Agency
ATTN: OSI/PSTD, Rm 5 F 19

Department of Commerce
National Bureau of Standards
ATTN: R. Moore

Department of Transportation
Office of the Secretary
ATTN: R. Lewis
ATTN: R. Doherty

Institute for Telecommunications Sciences
National Telecommunications & Info. Admin.
ATTN: L. Berry
ATTN: A. Jean
ATTN: W. Utlaut
ATTN: D. Crombie

National Oceanic & Atmospheric Admin.
Environmental Research Laboratories
Department of Commerce
ATTN: G. Reid
ATTN: R. Grubb

DEPARTMENT OF DEFENSE CONTRACTORS

Aerospace Corp.
ATTN: F. Morse

Analytical Systems Engineering Corp.
ATTN: Radio Sciences

Berkeley Research Associates, Inc.
ATTN: J. Workman

Boeing Co.
ATTN: J. Kenney
ATTN: G. Keister
ATTN: D. Murray
ATTN: G. Hall
ATTN: S. Tashird

University of California at San Diego
ATTN: H. Booker

Computer Sciences Corp.
ATTN: H. Blank

DEPARTMENT OF DEFENSE CONTRACTORS (Continued)

General Electric Co.
Space Division
ATTN: M. Bortner

General Electric Co.
ATTN: F. Reibert

General Electric Company-TEMPO
Center for Advanced Studies
ATTN: W. Knapp
ATTN: DASIAC
ATTN: B. Gambill

General Research Corp.
Santa Barbara Division
ATTN: J. Ise, Jr.
ATTN: J. Garbarino

Geophysical Institute
University of Alaska
ATTN: Technical Library

GTE Sylvania, Inc.
Electronics Systems Grp.-Eastern Div.
ATTN: M. Cross

Institute for Defense Analyses
ATTN: J. Aein

International Tel. & Telegraph Corp.
ATTN: Technical Library

JAYCOR
ATTN: S. Goldman

Johns Hopkins University
Applied Physics Lab.
ATTN: T. Potemra
ATTN: Document Librarian
ATTN: T. Evans

DEPARTMENT OF DEFENSE CONTRACTORS (Continued)

Science Applications, Inc.
ATTN: D. Sachs

SRI International
ATTN: G. Carpenter
ATTN: D. Neilson
ATTN: G. Price

Lawrence Livermore Laboratory
University of California
ATTN: Doc. Con. for Technical Information
Dept. Library

M.I.T. Lincoln Lab.
ATTN: D. Towle

Mission Research Corp.
ATTN: D. Sowle
ATTN: M. Scheibe

Mitre Corp.
ATTN: C. Callahan
ATTN: G. Harding

Mitre Corp.
ATTN: M. Horrocks

Pacific-Sierra Research Corp.
ATTN: E. Field, Jr.

R & D Associates
ATTN: R. Lelevier
ATTN: B. Gabbard

Rand Corp.
ATTN: C. Crain